ISSN 1063-7842, Technical Physics, 2021, Vol. 66, No. 6, pp. 896–902. © Pleiades Publishing, Ltd., 2021.
Russian Text © The Author(s), 2021, published in Zhurnal Tekhnicheskoi Fiziki, 2021, Vol. 91, No. 6, pp. 928–934.

GASES AND LIQUIDS

Ignition of Boron-Containing High-Energy Materials Based on an Oxidizer and Polymer Binder

A. G. Korotkikh[a, b,*], I. V. Sorokin[a], K. V. Slyusarskiy[a], and V. A. Arkhipov[b]

[a] *Tomsk Polytechnic University, Tomsk, 634050 Russia*
[b] *Tomsk State University, Tomsk, 634050 Russia*
**e-mail: korotkikh@tpu.ru*

Received November 28, 2020; revised January 22, 2021; accepted January 25, 2021

Abstract—The use of aluminum borides is a promising direction in the development of modern propellant compositions and aerial vehicles. We present experimental data on the kinetics of oxidation of microscale powders of aluminum, amorphous boron, and the aluminum borides AlB_2 and AlB_{12} in air upon heating at a constant rate of 10°C/min and the results of laser-assisted ignition of high-energy materials that contain these metal powders and are based on ammonium perchlorate, ammonium nitrate, and an inert binder or an energetic combustible binder. We show that the use of the boron-containing powders enables us to lower the onset temperature of oxidation and the temperature of intense oxidation, while increasing their oxidation effectiveness, compared to pure aluminum. The dependences of ignition delay time on the heat flux show that the AlB_2 and AlB_{12} powders are the most effective metal fuel components for solid propellants based on ammonium perchlorate, ammonium nitrate, and an energetic binder: they display the shortest ignition delay time and require the lowest heat input for ignition.

DOI: 10.1134/S1063784221060104

INTRODUCTION

Powered metals are high-energy components of modern composite solid and hybrid propellants [1] used in solid-propellant rocket engines and aerial vehicles. Aluminum powders with different degrees of dispersion are the most common metal fuel components in high-energy materials (HEMs) used in the aerospace industry [2]. Presently, seeking ways to increase the heat of combustion of HEMs by introducing boron-containing components is an important task. The specific heat of combustion of boron is 58.1 MJ/kg [3], which is considerably higher than that of aluminum (31 MJ/kg) [3, 4]. However, upon heating, when boron particles ignite, a compact layer of B_2O_3 oxide is formed on their surface [5], which prevents their complete oxidation at relatively low temperatures. Theoretically, the mass gain in complete oxidation of boron is around 218%. Thermal analysis shows that the mass gain observed on heating boron in oxygen to a temperature of 1000°C is ~140% [6], while heating boron in air to 1500°C yields a mass gain of ~160% [7]. The oxidation reactions, thus, involve no more than 75 and 82 wt % of the initial boron mass, respectively.

The use of different alloys based on Al–B (aluminum borides) [8–10] or aluminum/boron mechanical mixtures with different ratios between components [11–13] is a promising possibility to overcome drawbacks of boron and aluminum powders. Due to the development of new propulsion systems and aerial vehicles, it is relevant to use aluminum borides as combustible components of HEMs. These metal fuels are characterized by high density (2.50–2.84 g/cm^3), and their specific heat of combustion (43–54 MJ/kg [3]) is similar to that for boron. In addition, aluminum borides have been shown to display a superior reactivity on heating and during combustion process because of the presence of aluminum and boron in their composition and the absence of a refractory layer of Al_2O_3-oxide on the particle surface [12–14]. The use of aluminum borides may find broad application in high-energy composite propellants, because the extent of AlB_2 oxidation is ~80%, while that of the initial powdered boron and aluminum is ~20 and ~67%, respectively [15]. The specific heat of combustion of metal borides is 40–70% higher than that of pure aluminum [3]. Additionally, the combustion efficiency of compositions based on potassium perchlorate and polytetrafluoroethylene with the nanoscale powder AlB_2 was 5–20% higher than that of a composition with microscale aluminum diboride powder, as was established experimentally in [16]. We also note that interaction between Ti, Al and boron results in the release of a large amount of energy, which is foundational to self-propagating high-temperature synthesis (SHS) in boride metals [17, 18].

Table 1. HEM compositions under study

HEM composition	Components, wt %				α*
	AP (size, μm)	AN (size, μm)	Binder	Metal, type	
1-1	69.0 (165–315, <50)	–	16.0, SKDM-80	15.0, Al	0.50
1-2	74.0 (165–315, <50)	–	11.0, SKDM-80	15.0, B	0.50
1-3	71.4 (165–315, <50)	–	13.6, SKDM-80	15.0, AlB_2	0.50
1-4	73.2 (165–315, <50)	–	11.8, SKDM-80	15.0, AlB_{12}	0.50
2-1	21.3 (165–315)	49.8 (50–100)	13.9, SKDM-80	15.0, Al	0.50
2-2	22.5 (165–315)	52.5 (50–100)	10.0, SKDM-80	15.0, B	0.48
2-3	21.9 (165–315)	51.3 (50–100)	11.8, SKDM-80	15.0, AlB_2	0.50
2-4	22.5 (165–315)	52.5 (50–100)	10.0, SKDM-80	15.0, AlB_{12}	0.50
3-1	15.0 (160–315)	35.0 (<100)	20.0, MPVT-ASP	30.0, Al	0.66
3-2	18.0 (160–315)	42.0 (<100)	25.0, MPVT-ASP	15.0, B	0.65
3-3	15.6 (160–315)	36.4 (<100)	23.0, MPVT-ASP	25.0, AlB_2	0.57
3-4	17.7 (160–315)	40.3 (<100)	25.0, MPVT-ASP	17.0, AlB_{12}	0.63

*α is the coefficient showing the excess of oxidizer.

The aims of this work are (i) to determine the parameters of oxidation of microscale aluminum powder, amorphous boron, and aluminum borides (AlB_2 and AlB_{12}) from experimental data of thermal analysis; (ii) establish the ignition/combustion behavior; and (iii) determine the effect that boron, as part of an HEM composition, has on the ignition delay time in radiant heating of a propellant sample.

1. MATERIALS AND METHODS

1.1. HEM Compositions

In preparing HEM compositions, we used microscale powders of aluminum (mean particle diameter d_{43} = 10.8 μm), amorphous boron (d_{43} = 2.0 μm), and the aluminum borides AlB_2 (d_{43} = 6.2 μm) and AlB_{12} (d_{43} = 2.3 μm), which were obtained by SHS in an inert environment at the Research Institute for Applied Mathematics and Mechanics, Tomsk State University. The Al and B components taken in the specified ratio were compacted into cylindrically shaped samples using a hydraulic press and placed in an argon-filled SHS reactor. The metal samples sintered during SHS process were ground in a ball mill for 30 min. The phase composition of aluminum borides in the resulting powders, i.e., the final products, was analyzed on a Shimadzu XRD-6000B X-ray diffractometer with the result of 55.5 wt % Al and 44.5 wt % B in AlB_2 and 17.2 wt % Al and 82.8 wt % B in AlB_{12} [3]. To study the ignition behavior of HEM compositions, three-component compositions were prepared (Table 1), which contained ammonium perchlorate (AP) and grade SKDM-80 butadiene rubber resin (composition 1); AP, ammonium nitrate (AN), and SKDM-80 (composition 2); and AP, AN, and grade MPVT-ASP methyl polyvinyltetrazole (composition 3).

1.2. Experimental Units

The oxidation of powdered metals in air was investigated using an STA 449 F3 Jupiter thermal analyzer (Netzsch), which combines a thermogravimetric (TG) analysis and a differential scanning calorimetry (DSC). In carrying out thermal analysis, a sample of a powdered metal (with a weight of 5–8 mg) was placed in ceramic crucible. The sample was heated in the furnace from 30 to 1200°C at a liner rate of 10°C/min, while the air flow rate was 150 mL/min.

The key parameters characterizing the ignition of HEM compositions were determined on a test stand that included a continuous wave RLS-200 CO_2 laser with an operational wavelength of 10.6 μm and a maximum power of 200 W, an electrical power supply, cooling systems, and systems for recording the ignition parameters. The diameter of the laser beam exiting a half mirror of CO_2 laser was approximately equal to the sample diameter. HEM samples containing powdered metals had a diameter and height of 10 and 30 mm, respectively, and were fabricated by through-feed pressing followed by hardening in a dry oven; before experiments, they were cut into 5-mm-high tablets. The density of hardened HEM samples was 1.76–1.78 g/cm^3. The experimental unit has been described in detail elsewhere [10]. Ignition delay time t_{ign} for a test HEM composition was determined from the difference in electrical signals from the photodiodes registering the time moment at which the sample was initiated (opening of the electromagnetic valve) and the time moment at which flame appeared near to the

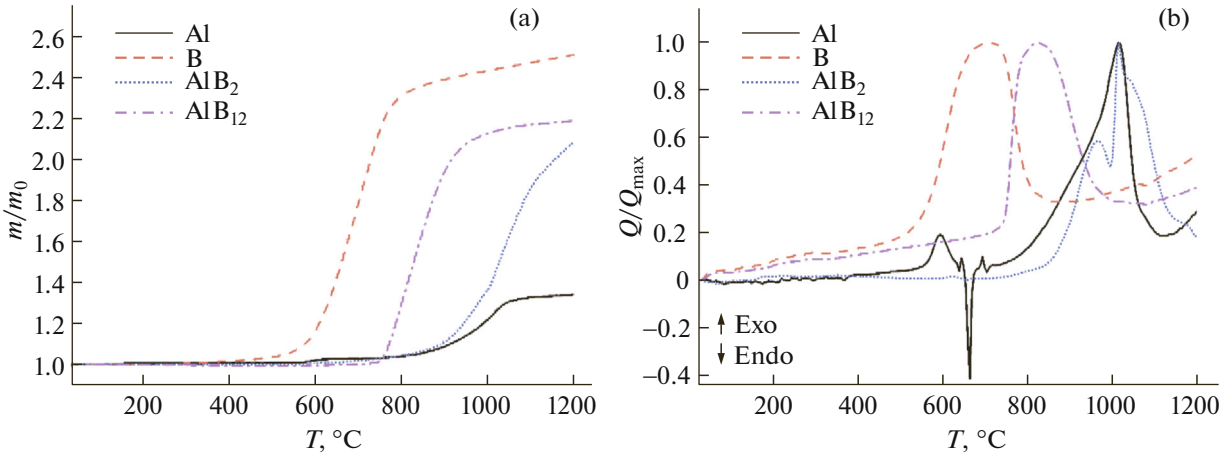

Fig. 1. (a) TG and (b) DSC curves for Al, B, AlB_2, and AlB_{12} powders recorded at a heating rate of 10°C/min in air.

propellant surface. In experiments, the heat flux incident on the end side of a sample was varied in the range of $q = 60–220$ W/cm^2. The output power of laser beam was adjusted by means of the control system of pulse pumping parameters and the high-frequency power of discharge electrodes of the laser head block. The relative error of scattering of delay time t_{ign} was in the range of 5–15% at a confidence level of 0.95.

2. RESULTS AND DISCUSSION

2.1. Thermal Analysis

TG and DSC analyses registered the variation of relative mass (Fig. 1a) and the specific heat flux (Fig. 1b) for Al, B, AlB_2, and AlB_{12} powders.

Upon heating a sample of microscale Al powder in air, the oxidation process occurs in two stages. The first oxidation stage takes place before the aluminum melts in the temperature range of 560–640°C and is accompanied by a slight increase in sample mass (~2%). The aluminum powder melts endothermically at 660°C (Fig. 1b), at 800–1060°C which is followed by a marked increase in the sample mass (up to 34%; the second stage) and, simultaneously, intense heat release ($Q_{max} = 11.9$ W/g).

Upon heating amorphous boron or aluminum boride powders, the oxidation process occurs in one stage (Fig. 1). For a sample of amorphous boron powder, intense oxidation occurs in the temperature range of 560–800°C and the maximum specific heat flux is $Q_{max} = 27.7$ W/g, with the boron mass increasing by 140% (relative to the initial mass of amorphous boron sample; Fig. 1a). Upon heating the boron powder in air further, to a temperature of 1200°C, the process becomes less intense, and the sample mass gradually increases by ~10%.

TG and DCS curves for AlB_2 powder (Fig. 1) show that the diboride oxidation is shifted toward higher temperatures as a result of its large aluminum content (compared to AlB_{12} and B). The AlB_2 powder undergoes intense oxidation in the temperature range of 880–1120°C, and the maximum specific heat flux is 10.6 W/g, with the sample mass increasing by 108%. The presence of two peaks on the DSC curve for AlB_2 powder at temperatures of 960 and 1010°C (Fig. 1b) may suggest that it is unstable and undergoes decomposition at a temperature above 900°C to yield aluminum and AlB_{12} or other boride phases and boron and aluminum alloys, as was observed in [19, 20].

As does amorphous boron, aluminum dodecaboride powder (AlB_{12}) oxidizes in one stage (Fig. 1), but its intense oxidation occurs at higher temperatures, i.e., 750–950°C, and the maximum heat flux is 28.9 W/g. Upon heating to 1200°C in air, the mass of the AlB_{12} sample increases by 118%.

Experimental data obtained from TG–DSC analyses of the considered metal powders enabled us to determine onset temperature T_{on} of intense oxidation, mass gain Δm, total heat Q of the oxidation, and oxidation rate v_{ox} (Table 2).

Amorphous boron powder displayed the highest heat of oxidation in air ($Q = 21\,550$ J/g), among the other powders under study. AlB_{12} powder displayed the highest oxidation rate in the temperature range of 780–870°C: $v_{ox} = 0.624$ μg/min.

Earlier calculations of oxidation kinetic parameters [21] showed that the activation energy of aluminum and aluminum diboride powders reach the highest values (300–370 kJ/mol) at an oxidation conversion of 0.10–0.25, while the activation energy for boron and aluminum dodecaboride powders varied in the range of 50–200 kJ/mol at the same degree of conversion. The activation energy of Al powder in the range of degree of conversion of 0.4–0.8 is much higher (300–450 kJ/mol) than activation energy for amorphous

Table 2. Parameters of oxidation of metal and boron powders

Powder	T_{on}, °C	Δm, wt %	Q, J/g	v_{ox}, mg/min (in the temperature range, °C)
Al	800	34	3680	0.119 (970–1040)
B	560	150	21550	0.534 (650–750)
AlB_2	880	108	5230	0.306 (1000–1080)
AlB_{12}	750	118	20270	0.624 (780–870)

boron, AlB_2, and AlB_{12}, which fall in the ranges of 120–350, 200–250, and 50–90 kJ/mol, respectively.

In the range of degree of conversion of 0.2–0.8, aluminum dodecaboride (AlB_{12}) powder displays the lowest activation energy of oxidation compared to Al, B, and AlB_2 powders. However, at the degree of conversion of 0.1–0.2, which is more adequate to the process of powder ignition, the activation energy value for AlB_{12} is lower than for powdered boron.

2.2. Ignition Delay Time

For the considered HEM compositions, which contain metal powders, the ignition delay time was determined as a function of heat flux upon initiation of samples with a laser pulse (data points in Fig. 2). Snapshots from high-speed video recording of ignition of HEM composition 3 (contains AP, AN, and MPVT-ASP) that was initiated by radiant heat with flux $q = 68$ W/cm^2 are presented in Fig. 3. The values for fitting parameters for power-law dependence $t_{ign}(q)$ and coefficient K_{ign}, the latter being the ratio between the ignition delay time of Al-based HEM and the ignition delay time of the HEM containing B, AlB_2, or AlB_{12}, are summarized in Tables 3 and 4.

The analysis of our experimental data shows that composition 1, which is based on AP/SKDM-80/Me, has the shortest ignition time, whereas composition 3, which is based on AP/AN/MPVT-ASP/Me, has the longest ignition time under the same ignition conditions and for the same content of metal fuel component. The ignition delay time for composition 1-1, which contains pure Al, is 3.0–4.1 times shorter than t_{ign} for composition 3-1 (Fig. 2a), meaning that the presence of an energetic binder in the HEM considerably increases the heating and ignition time compared to a HEM containing an inert binder. Substituting the mixture of oxides AP/AN (composition 2-1) for pure

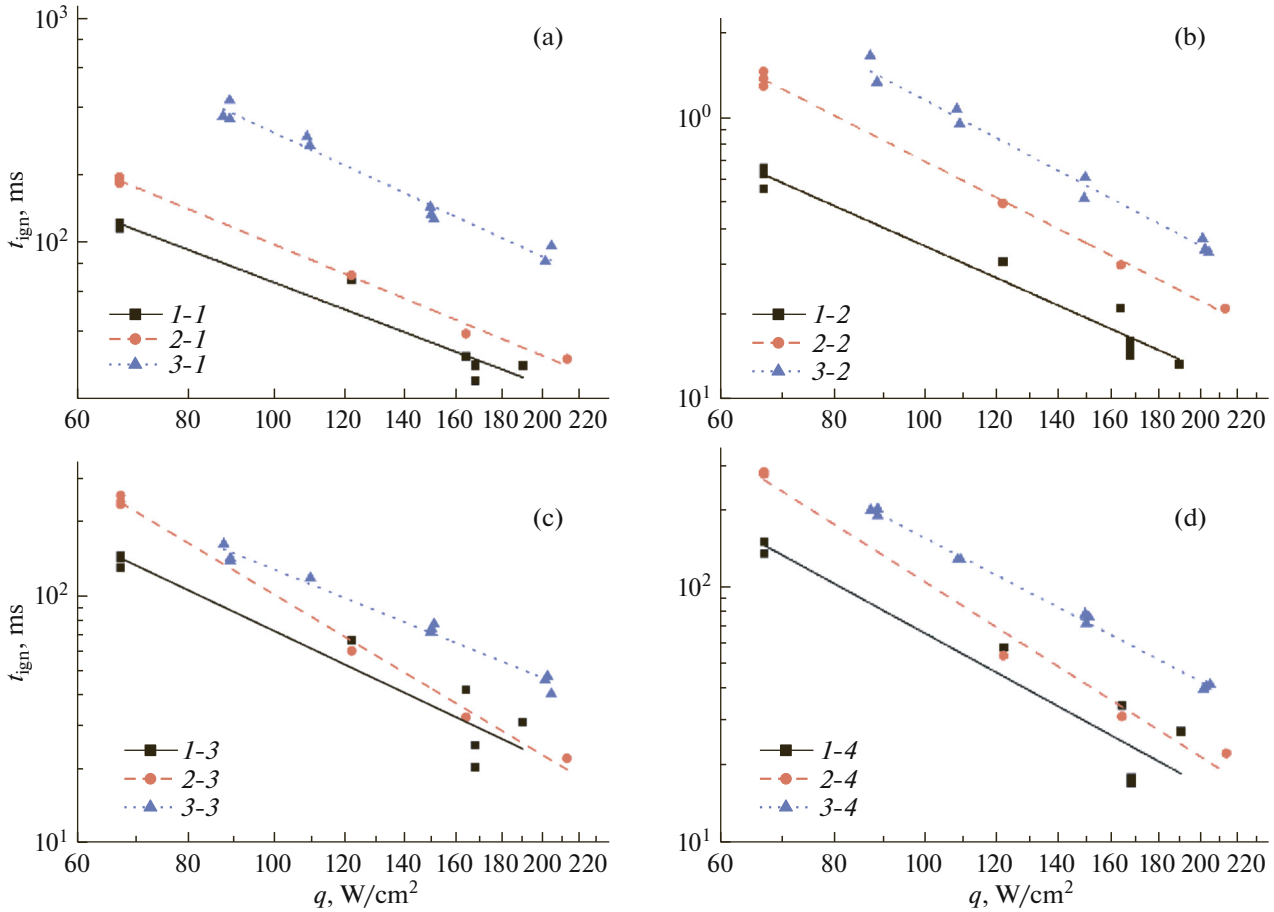

Fig. 2. Ignition delay time as a function of the heat flux for HEM compositions: (a) 1-1, 2-1, 3-1 with Al; (b) 1-2, 2-2, 3-2 with B; (c) 1-3, 2-3, 3-3 with AlB_2; and (d) 1-4, 2-4, 3-4 with AlB_{12}.

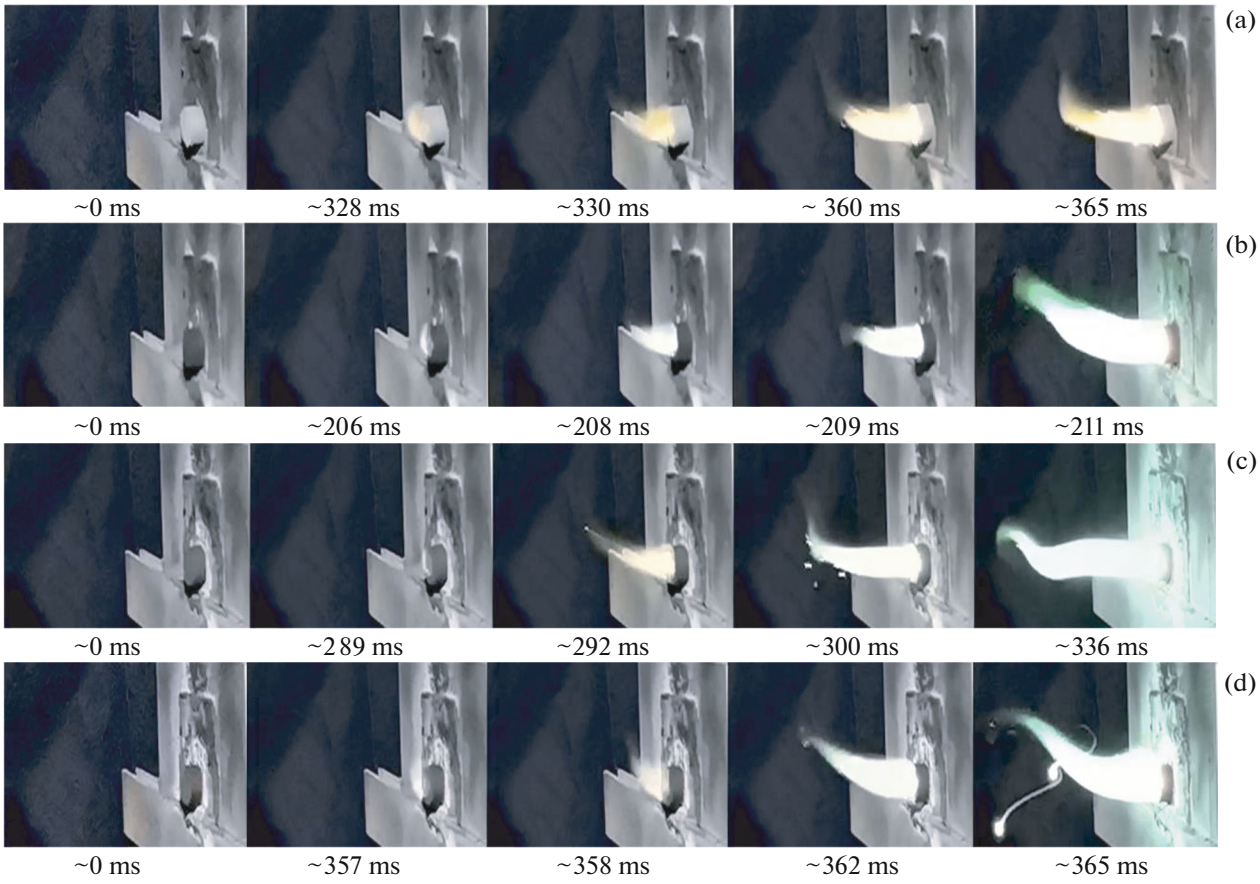

Fig. 3. Snapshots from high-speed video recording of ignition of HEMs based on AP/AN/MPVT-ASP and containing (a) Al, (b) B, (c) AlB_2, and (d) AlB_{12}. Conditions: $q = 68$ W/cm^2.

AP (composition 1-1) in the HEM composition based on the inert binder SKDM-80 makes time t_{ign} longer by a factor of 1.1–1.7 under the same ignition conditions.

With amorphous boron substituting for Al powder in all the HEM compositions under study, the ignition delay times became shorter in the entire q range. That being so, the ratio of t_{ign} for composition 3-2, which is based on AP/AN/MPVT, to t_{ign} for composition 1-2, which is based on AP/SKDM-80 and contains pure boron, is 2.5–2.9, depending on specific q values (Fig. 2b).

The ratio of t_{ign} for composition 2-2, which is based on AP/AN/SKDM-80, to t_{ign} for composition 1-2, which is based on AP/SKDM-80 and contains boron, is 1.4–2.1.

In the presence of AlB_2 in composition 1-3, which is based on AP/SKDM-80, t_{ign} become shorter by a factor of 1.2–1.9 and 1.4–1.8 compared to compositions 2-3 (AP/AN/SKDM-80) and 3-3 (AP/AN/MPVT), respectively (Fig. 2c). A typical situation was observed for HEM compositions 1-4, 2-4, and 3-4, which contain the AlB_{12} (Fig. 2d).

For HEM compositions based on SKDM-80 butadiene rubber resin, AP, or AP/AN (compositions 1 and 2), substitution of aluminum borides AlB_2 and AlB_{12} for Al leads to ignition delay time t_{ign} being longer by 2–20% at heat flux densities $q \le 110$ W/cm^2 (Table 3). For $q > 160$ W/cm^2, the ignition delay time

Table 3. Values a and b of the fitting equation $t_{ign}(q) = aq^{-b}$ for HEM compositions containing metal powders

HEM	1-1	1-2	1-3	1-4	2-1	2-2	2-3	2-4	3-1	3-2	3-3	3-4
$a \times 10^{-4}$	6.92	2.77	18.3	58.1	18.7	14.0	199	385	142	32.1	10.0	87.4
b	1.51	1.45	1.70	1.97	1.64	1.65	2.15	2.28	1.83	1.72	1.45	1.87

Table 4. Coefficient K_{ign} calculated for HEM compositions depending on heat flux

HEM composition	K_{ign}								
	1	2	3	1	2	3	1	2	3
q, W/cm^2	t_{ing}^{Al}/t_{ing}^{B}			$t_{ing}^{Al}/t_{ing}^{AlB_2}$			$t_{ing}^{Al}/t_{ing}^{B_{12}}$		
70	1.92	1.38	2.76	0.85	0.80	2.75	0.84	0.73	1.93
110	1.87	1.39	2.63	0.93	1.01	2.31	1.03	0.98	1.96
150	1.83	1.39	2.54	0.98	1.18	2.05	1.19	1.19	1.99
210	1.80	1.39	2.45	1.05	1.40	1.80	1.39	1.48	2.02

of the indicated HEM composition becomes shorter. We note that, in the presence of amorphous boron in compositions 1 and 2, the ignition delay time of the SKDM-80-based HEMs become shorter by a factor of 1.9 and 1.4, respectively, in the entire range of heat flux density.

In the presence of AlB_2 and AlB_{12} aluminum borides in composition 3, the ignition delay times of HEMs based on an energetic binder and AP/AN became considerably shorter compared to HEMs containing pure Al—by a factor of 1.8–2.8, depending on q values.

According to our infrared imaging data, a dramatic rise in the temperature across the entire area of the end surface and an increase in the rate of removal of reaction products occurred at the moment when the decomposition products were removed from the surface of a propellant sample and flame emerged, which was due to additional heat flux from the chemical reaction zone in the gas phase. The decomposition products carry powder particles off the surface of reaction layer, which creates additional heat flux due to exothermic oxidation of metal particles. We note that the heat-up period and the formation period of fuel reaction layer for the HEM containing pure aluminum is fairly long compared to other HEM compositions containing boron or the aluminum borides and that a major fraction of the heat supplied from the radiation source is consumed for conduction heating of the surface layer, decomposition of the components, and melting of aluminum particles located close to the sample surface. The presence of a considerable fraction of coarse particles in the Al powder and a refractory oxide layer at its surface contribute to an increase in the onset temperature of its intense oxidation compared to amorphous boron or AlB_{12}, which results in reduced ignition stability of the sample and less heat released due to oxidation of particles near the propellant surface. Additionally, we hypothesize that the boron powder increases the absorbing capacity of the propellant surface, thereby shortening the ignition delay time of a HEM.

CONCLUSIONS

We performed TG–DSC analyses of microscale aluminum, boron, and aluminum boride powders in the temperature range of 30–1200°C in air. From the thermal analysis data, we determined the onset temperature of oxidation, the mass gain, the heat of oxidation reaction, and the maximum oxidation rate of the metal and boron powders. The oxidation of aluminum proceeds in two stages. The first stage occurs below the melting point of aluminum and does not make a significant contribution (the mass gain is ~2%). The main process of aluminum oxidation occurs in the temperature range of 800–1060°C. Boron and the aluminum boride powders undergo a single-stage oxidation. We note that a small endothermic peak is observed in the case of aluminum diboride, which is related to the process of AlB_2 decomposition and the formation of other boride phases and aluminum–boron alloys at air temperatures of 965 and 1013°C.

Amorphous boron powder and aluminum dodecaboride powder have the highest specific heats of oxidation (21.6 and 20.3 kJ/g, respectively), which are much higher than those of Al (3.7 kJ/g) or AlB_2 (5.2 kJ/g). The highest oxidation rate was registered for AlB_{12}, which was 15% higher than the value for B and exceeded the values for AlB_2 and Al powders by a factor of 2.0 and 5.2, respectively.

Our experimental investigation of ignition process of HEM compositions containing Al, B, AlB_2, or AlB_{12} showed that the presence of AP/AN double oxidizer and the MPVT-ASP energetic binder in HEM composition makes the ignition delay time longer compared to HEM based on AP and SKDM-80 butadiene rubber resin.

The substitution of amorphous boron for microscale aluminum leads to shorter ignition delay time for all the considered HEM compositions. The highest effectiveness due to the substitution of AlB_2 and AlB_{12} for Al was found for the HEM composition based on the double oxidizer and an energetic binder (i.e., AP/AN/MPVT-ASP), which improved ignition stability and shortened the ignition delay time by a factor of 1.8–2.8, provided that the heat flux was the same. For the HEM compositions with AlB_2 or AlB_{12}

and an inert binder (i.e., AP/SKDM-80 and AP/NA/SKDM-80), the heat-up time and ignition delay time of the propellants become shorter at heat flux of $q > 160$ W/cm^2.

FUNDING

This work was supported by the Russian Foundation for Basic Research, project no. 20-03-00588.

CONFLICT OF INTEREST

The authors declare that they have no conflicts of interest.

REFERENCES

1. E. L. Dreizin, Prog. Energy Combust. Sci. **35** (2), 141 (2009). https://doi.org/10.1016/j.pecs.2008.09.001
2. A. Gromov, L. T. Deluca, A. P. Il'in, U. Teipel, A. Petrova, and D. Prokopiev, Int. J. Energ. Mater. Chem. Propul. **13** (5), 399 (2014). https://doi.org/10.1615/IntJEnergeticMaterialsChemProp.2014011255
3. *Energy-Intensive Fuels for Aviation and Rocket Engines*, Ed. by L. S. Yanovskii (Fizmatlit, Moscow, 2009) [in Russian].
4. D. S. Sundaram, V. Yang, and V. E. Zarko, Combust., Explos. Shock Waves **51** (2), 173 (2015). https://doi.org/10.1134/S0010508215020045
5. Y. Sun, K. L. Chintersingh, M. Schoenitz, and E. L. Dreizin, J. Phys. Chem. C **123** (18), 11807 (2019). https://doi.org/10.1021/acs.jpcc.9b03363
6. X. Liu, J. Gonzales, M. Schoenitz, and E. L. Dreizin, Thermochim. Acta **652**, 17 (2017).
7. D. Yu, C. Kong, J.-K. Zhuo, S. Q. Li, and Q. Yao, Sci. China: Technol. Sci. **58** (12), 2016 (2015). https://doi.org/10.1007/s11431-015-5841-0
8. V. Arkhipov, L. Savelieva, and P. Ponomarev, MATEC Web Conf. **110**, 01075 (2017). https://doi.org/10.1051/matecconf/201711001075
9. V. A. Arkhipov, A. S. Zhukov, V. T. Kuznetsov, N. N. Zolotorev, N. A. Osipova, and K. G. Perfil'eva, Combust., Explos. Shock Waves **54** (6), 689 (2018). https://doi.org/10.1134/S0010508218060084
10. A. G. Korotkikh, V. A. Arkhipov, I. V. Sorokin, and E. A. Selikhova, Khim. Fiz. Mezoskop. **20** (1), 5 (2018).
11. M. L. Whittaker, R. A. Cutler, and P. E. Anderson, MRS Online Proc. Libr. **1405**, 96 (2011). https://doi.org/10.1557/opl.2012.64
12. D. Liang, R. Xiao, J. Liu, and Y. Wang, Aerosp. Sci. Technol. **84**, 1081 (2019).
13. S. Adil and B. S. Murty, Thermochim. Acta **678**, 178306 (2019).
14. M. L. Whittaker, H. Y. Sohn, and R. A. Cutler, J. Solid State Chem. **207**, 163 (2013).
15. I. Zhukov, A. Vorozhtsov, V. Promakhov, Y. Dubkova, A. Zhukov, and A. Khrustalev, MATEC Web Conf. **243** (00015), 1 (2018). https://doi.org/10.1051/matecconf/201824300015
16. D. A. Yagodnikov, A. V. Voronetskii, and V. I. Sarab'ev, Combust., Explos. Shock Waves **52** (3), 300 (2016). https://doi.org/10.1134/S0010508216030072
17. V. V. Promakhov, M. Kh. Ziatdinov, I. A. Zhukov, S. A. Vorozhtsov, A. E. Matveev, and S. S. Titov, Polzunov. Vestn., No. 4-1, 76 (2016).
18. I. A. Zhukov, M. K. Ziatdinov, A. B. Vorozhtsov, A. S. Zhukov, S. A. Vorozhtsov, and V. V. Promakhov, Russ. Phys. J. **59** (8), 1324 (2016). https://doi.org/10.1007/s11182-016-0911-8
19. S. L. Guseinov, S. G. Fedorov, A. Y. Tuzov, S. I. Malashin, A. I. Drachev, M. R. Kisilev, B. V. Pevchenko, and O. V. Voron'ko, Nanotechnol. Russia **10** (5–6), 420 (2015). https://doi.org/10.1134/S199507801503009X
20. N. V. Kirillova, A. I. Kharlamov, and S. V. Loichenko, Inorg. Mater. **36** (8), 776 (2000). https://doi.org/10.1007/BF02758596
21. A. G. Korotkikh, K. V. Slyusarskii, and I. V. Sorokin, Khim. Fiz. Mezoskop. **22** (2), 164 (2020). https://doi.org/10.15350/17270529.2020.2.16

Translated by A. Kukharuk